MATERIALS CHEMISTRY FRONTIERS

CHINESE CHEMICAL SOCIETY

ROYAL SOCIETY OF CHEMISTRY

RESEARCH ARTICLE

View Article Online
View Journal | View Issue

Cite this: *Mater. Chem. Front.*, 2021, **5**, 876

Developing D–π–D hole-transport materials for perovskite solar cells: the effect of the π-bridge on device performance†

Yangmei Ou,‡[a] Anxin Sun,‡[a] Haibei Li,[b] Tai Wu,[a] Dongyang Zhang,[a] Peng Xu,[a] Rongmei Zhao,[a] Liqiong Zhu,[a] Runtao Wang,[a] Bo Xu,*[c] Yong Hua*[a] and Liming Ding*[d]

Received 16th September 2020,
Accepted 5th November 2020

DOI: 10.1039/d0qm00719f

rsc.li/frontiers-materials

Three cost-effective D–π–D hole transport materials (HTMs) with different π-bridges, including biphenyl (**SY1**), phenanthrene (**SY2**), and pyrene (**SY3**), have been synthesized *via* a one-pot reaction with cheap commercially available starting materials for application in organic–inorganic hybrid perovskite solar cells (PSCs). The effects of the various π-bridges on the photophysical, electrochemical, and electrical properties, and film morphologies of the materials, as well as on the photovoltaic properties of the PSCs, have been systematically investigated accordingly. Our results clearly show that HTM-**SY3** with pyrene as the π-bridge exhibits higher hole mobility and better hole extraction/transport and film formation abilities than the other two HTMs. Devices that employed **SY3** as the HTM show impressive power conversion efficiency (PCE) values of 19.08% and 13.41% in $(FAPbI_3)_{0.85}(MAPbBr_3)_{0.15}$- and $CsPbI_2Br$-based PSCs, respectively, which are higher than those of the reference HTM-**SY1**- and **SY2**-based ones. Our studies demonstrate a promising strategy to rationally design and synthesize low-cost and efficient HTMs through structural engineering for use in PSCs.

1. Introduction

Solution-processed metal halide perovskite solar cells (PSCs) have been demonstrated to be one of the most promising solar technologies owing to their low production cost and high photovoltaic performance.[1–7] Since the pioneering work reported by Miyasaka *et al.* in 2009,[8] perovskite-based light harvesting materials have attracted wide attention from scientists both in academia and industry, due to their extraordinary optoelectrical characteristics, including a wide light absorption spectrum from visible to near-infrared, tunable band-gap energy, long electron–hole diffusion lengths, ambipolar charge-transport capability, and high charge-carrier mobility.[9–16] Benefitting from the tremendous efforts made towards new deposition method exploitations, device architecture optimization, and interface/additives engineering,[17–22] the certified record power conversion efficiency (PCE) of a single-junction PSC has been rapidly boosted to 25% just in a decade.[23] Generally, highly efficient PSCs possess a light-harvesting perovskite layer sandwiched between an electron transport material layer (ETM) and a hole transport material layer (HTM). Solution processable organic HTMs are of great significance to extract and transport photogenerated holes from the perovskite absorber at the perovskite/HTM interface and further improve the solar cell performance.[24–26]

Moreover, compact and uniform hole transport layers can usually act as a moisture barrier against the degradation of perovskite film under ambient conditions, enhancing the stability of PSCs.[27–30] So far, 2,2′,7,7′-tetrakis-(*N*,*N*-di-*p*-methoxy-phenyl-amine)-9,9′spiro-bifluorene (Spiro-OMeTAD) has been proven to be the most efficient and commonly used HTM in highly efficient PSCs due to its amorphous nature, high solubility in organic solvents, matched molecular frontier orbital energy and outstanding film forming ability.[31–34] Unfortunately, the preparation of Spiro-OMeTAD involves tedious and low-yielding synthetic protocols as well as costly multi-step purification, which makes it prohibitively expensive and thus inhibits its potential for industrial-scale applications. Besides, it is well-known that Spiro-OMeTAD exhibits relatively low hole-mobility around $\sim 10^{-6}$ cm^2 V^{-1} s^{-1} in the pristine state,[35]

[a] *Yunnan Key Laboratory for Micro/Nano Materials & Technology, School of Materials and Energy, Yunnan University, Kunming 650091, China. E-mail: huayong@ynu.edu.cn*
[b] *School of Ocean, Shandong University, Weihai 264209, China*
[c] *School of Chemistry, KTH-Royal Institute of Technology, SE-100 44, Sweden. E-mail: box@kth.se*
[d] *Center for Excellence in Nanoscience (CAS), Key Laboratory of Nanosystem and Hierarchical Fabrication (CAS), National Center for Nanoscience and Technology, Beijing 100190, China. E-mail: ding@nanoctr.cn*

† Electronic supplementary information (ESI) available. See DOI: 10.1039/d0qm00719f

‡ Yangmei Ou and Anxin Sun contributed equally to this work.

which results in low hole extracting/transporting efficiency in PSCs devices. Therefore, the aforementioned shortcomings make it highly desirable to develop efficient HTM candidates with facile synthetic routes and high hole-mobility to replace the commonly used Spiro-OMeTAD.

It has been reported that organic semiconducting materials adopting a donor–π bridge–donor (D–π–D) structure show excellent hole-transporting properties in the organic photovoltaic community due to the strong intermolecular π–π stacking interaction in solid-state thin films. Additionally, the interaction and hole transport properties can be finely modulated through tuning the π-conjugation within the resultant molecules.[36,37] These features have encouraged researchers to design and synthesize D–π–D typed organic molecules-based HTMs for PSCs applications.[38–40] However, the structure–property relationships of HTMs and the effects of the various π-conjugations of D–π–D HTMs on the PSCs photovoltaic properties have not been well-established yet. Herein, three novel D–π–D HTMs (named **SY1**, **SY2** and **SY3**) featuring diphenylamine as the donor along with biphenyl, phenanthrene or pyrene as the π-conjugation core units were designed and synthesized for comparison, as shown in Fig. 1. We systematically investigate the effect of varying the π-conjugated spacers of HTMs on the optoelectronic and hole transport properties as well as the related solar cell performances. Our results clearly show that the subtle structural change modification in the chemical structure of HTMs induced a significant influence on PSC performance.

2. Experimental

In this study, the molecular structures of **SY1**, **SY2** and **SY3** are shown in Fig. 1. The synthetic route (Scheme S1, ESI†) towards the target molecules only requires one step with high yield and cheap commercially available starting materials, which is much simpler than the preparation procedure of Spiro-OMeTAD (five steps).[41] The synthesis and device fabrication details are described in the ESI.† The final molecules were identified by NMR and high resolution MALDI-TOF, and the analytical data for all HTMs are in good agreement with the formulated structures. The thermal properties of HTMs were studied by thermogravimetric analysis (TGA) and differential scanning calorimetry (DSC). As shown in Fig. S6a (ESI†), the decomposition temperatures (T_d) of **SY1**, **SY2** and **SY3** are 315 °C, 351 °C and 382 °C, respectively, indicating that these HTMs possess good thermal stability. Additionally, the crystallization process from the DSC curves (Fig. S6b, ESI†) was detected at 193 °C, 202 °C and 338 °C for **SY1**, **SY2** and **SY3**, respectively, during the heating scan, while no crystallization was observed during the cooling step. These results clearly indicate that **SY3** exhibits better amorphous thin-film stability than **SY1** and **SY2** upon heating.

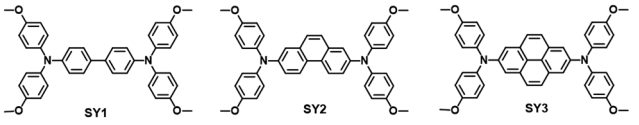

Fig. 1 The chemical structures of the HTMs.

3. Results and discussion

3.1. Optical and electrochemical properties

The normalized UV-vis absorption spectra of **SY1**, **SY2** and **SY3** measured in CH_2Cl_2 solution are shown in Fig. 2 and their spectroscopic data are compiled in Table 1. All of these HTMs exhibited a major broad absorption band in the range of 200–450 nm. The maximum absorption peaks (λ_{max}) of **SY1**, **SY2** and **SY3** are located at 353 nm, 366 nm, and 462 nm, respectively. It is noted that the maximum absorption increases gradually with the π-bridges varying from biphenyl to phenanthrene and then to pyrene due to more extended π-conjugation of the central scaffold, resulting in a more effective intramolecular charge transfer (ICT) effect.[42] Obviously, the three HTMs exhibit a weak absorption capacity in the visible region, thus they would not compete with the perovskite layer for light absorption in the PSC devices. The electronic features of the three HTMs were estimated by cyclic voltammetry (CV) (Fig. 2b) in CH_2Cl_2 solution and the corresponding data are listed in Table 1. As shown in Fig. 2c, the three HTMs exhibit reversible oxidation waves, indicating the good electrochemical stability. The highest occupied molecular orbital (HOMO) energy level of **SY1**, **SY2** and **SY3** is estimated to be −5.23 eV, −5.22 eV and −5.25 eV, respectively, which are sufficiently more positive than the valence band of the perovskite (−5.65 eV), indicating that the three HTMs are favorable for effectively extracting holes from the perovskite layer toward the Au counter electrode.[43,44] The lowest occupied molecular orbital (LUMO) energy levels of **SY1** (−2.13 eV), **SY2** (−2.29 eV) and **SY3** (−2.74 eV) are much higher than the value of the perovskite conduction band, which is expected to effectively block the undesired electron back-transfer from the perovskite layer to the Au electrode.

3.2. DFT calculations and hole mobility

To better understand the geometric and electronic properties of HTMs, density functional theory (DFT) calculations were conducted using the Gaussian 03 program package at the B3LYP/6-31+G(d) level. As depicted in Fig. 3, the electrons of the highest occupied molecular orbitals (HOMO) of the three HTMs are almost delocalized over the whole molecule, while the lowest unoccupied molecular orbitals (LUMO) are mainly localized at the π-bridges. Clearly, the good overlap between the HOMO and LUMO orbitals on the π-bridges suggests that the three materials may exhibit good intermolecular hole-transport ability in the HTM film state.[38,45] In addition, the calculated hole reorganization energy (E_R) values of the three materials are 215.52, 170.71 and 150.32 meV, respectively, which are much smaller than Spiro-OMeTAD (495 meV),[46] indicating that these materials are promising HTMs for PSCs applications. The hole-mobility of HTM thin-film is one of the significant factors that influence PSCs' performance. Therefore, the space-charge-limited current (SCLC) method was employed to study the

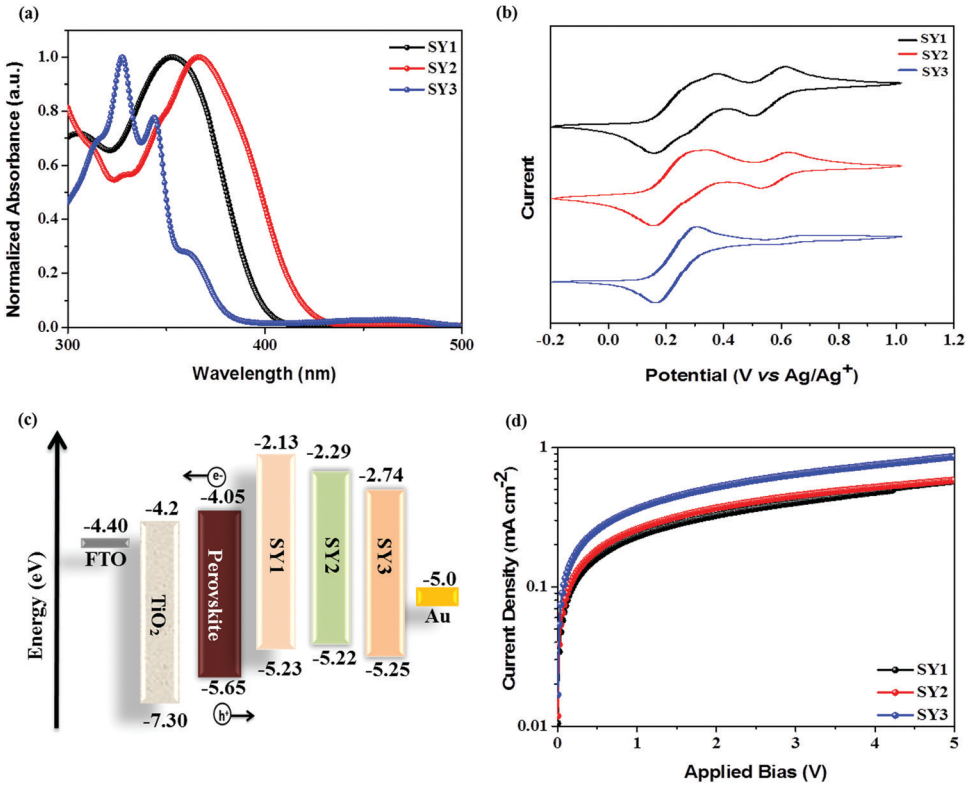

Fig. 2 (a) Normalized UV-vis absorption spectra of HTMs in CH_2Cl_2 solution. (b) Cyclic voltammetry (CV) curves of the HTMs. (c) An energy level diagram of the PSCs. (d) *J*–*V* curves obtained from hole-only ITO/PEDOT:PSS/HTMs/Au devices.

Table 1 The detailed physical parameters of **SY1**, **SY2**, and **SY3**

HTM	λ_{max}[a] (nm)	E_g^{opt}[b] (eV)	E_{HOMO}[c] (eV)	E_{LUMO}[d] (eV)	Hole mobility[e] ($cm^2\ V^{-1}\ s^{-1}$)	E_R[f] [meV]
SY1	353	3.10	−5.23	−2.13	1.62×10^{-4}	215
SY2	366	2.93	−5.22	−2.29	1.78×10^{-4}	170
SY3	462	2.51	−5.25	−2.74	2.18×10^{-4}	150

[a] Measured in CH_2Cl_2 solution. [b] Optical bandgap was calculated from the formula $1240/\lambda_{onset}$. [c] Using cyclic voltammetry in CH_2Cl_2 solution. [d] $E_{LUMO} = E_{HOMO} + E_{gap}$. [e] Hole mobility of HTM. [f] Hole reorganization energy.

influence of π-bridges on the hole-mobility of HTMs, as displayed in the Fig. 2d. The evaluated mobility values of **SY1**, **SY2** and **SY3** were determined to be 1.62×10^{-4} $cm^2\ V^{-1}\ s^{-1}$, 1.78×10^{-4} $cm^2\ V^{-1}\ s^{-1}$ and 2.18×10^{-4} $cm^2\ V^{-1}\ s^{-1}$, respectively, it is clear that the mobility value is strongly affected by the introduction of different π-bridges in the HTMs molecules, in the following order: **SY1** < **SY2** < **SY3**, this result reveals that more extended π-conjugation can be beneficial to enhancement of the hole transporting properties of the HTMs. As shown in Fig. S7 (ESI†), dopant-free **SY3** shows a comparable value of 1.12×10^{-5} $cm^2\ V^{-1}\ s^{-1}$ to that of Spiro-OMeTAD.[32] The above-mentioned results demonstrate that **SY3** is a promising HTM candidate for efficient PSCs.

3.3. Photovoltaic performance

The photocurrent density–voltage (*J*–*V*) characteristics of PSCs devices based on these HTMs (FTO/c-TiO_2/meso-TiO_2/$(FAPbI_3)_{0.85}(MAPbBr_3)_{0.15}$/HTM/Au) were evaluated under AM 1.5 G irradiation at 100 mW cm^{-2} and the curves are shown in Fig. 4a. The PSCs device fabricated with **SY1** exhibits an open-circuit voltage (V_{oc}) of 1.095 V, a short circuit current density (J_{sc}) of 21.69 mA cm^{-2} and a fill factor (FF) of 0.735, resulting in a PCE of 17.46%. **SY2** based PSCs provide a V_{oc} of 1.099 V, a J_{sc} of 22.55 mA cm^{-2} and a FF of 0.746, corresponding to a PCE of 18.49%. Upon the incorporation of the pyrene unit instead of the phenanthrene unit as the central π-bridge, PSCs based on **SY3** offer a V_{oc} of 1.114 V, a J_{sc} of 22.62 mA cm^{-2} and a FF of 0.757, yielding a high PCE of 19.08%, which is in comparison with the efficiency of Spiro-OMeTAD-based devices (19.44%). Moreover, the dopant-free **SY3**-based device gave a PCE of 16.67% with a J_{sc} of 21.46 mA cm^{-2}, a V_{oc} of 1.108 V and a FF of 0.701 (Fig. S10, ESI†). As shown in Fig. 4b, the integrated J_{sc} values of **SY1**, **SY2** and **SY3**-based PSCs calculated from the corresponding incident photon-to-electron conversion efficient (IPCE) spectra were 20.85, 21.59 and 21.98 mA cm^{-2}, respectively, which are consistent with the change trend of the

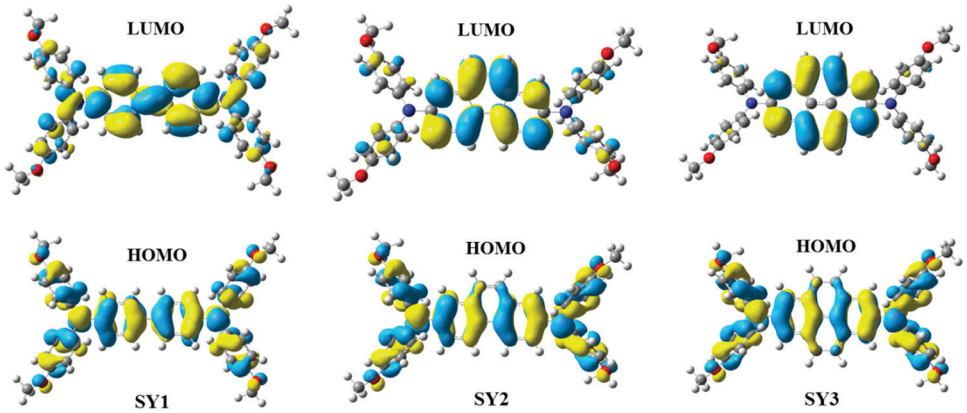

Fig. 3 The HOMO/LUMO distributions of the HTMs.

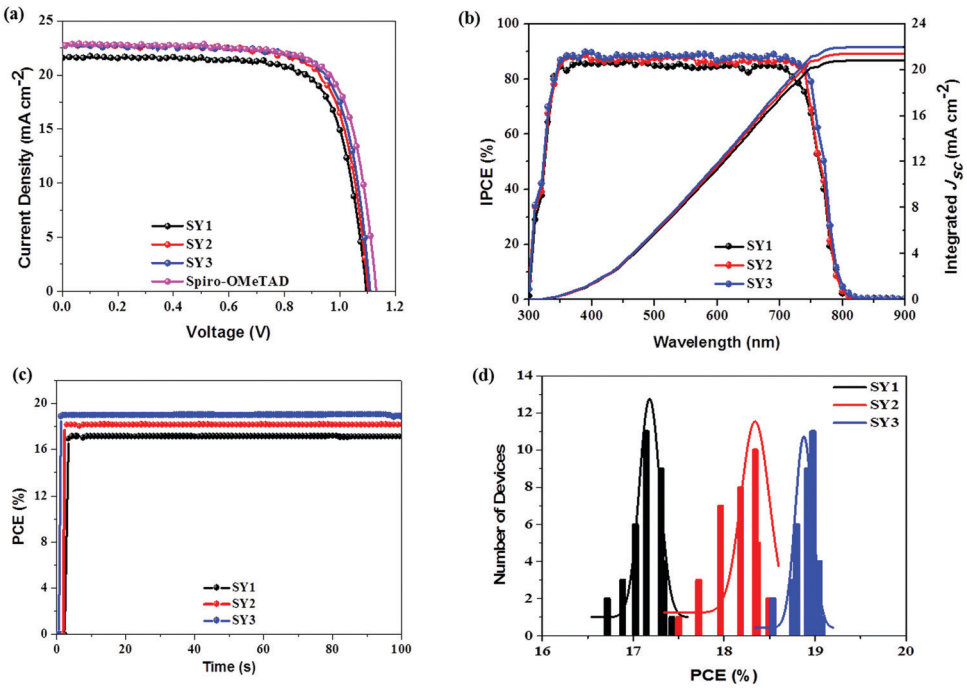

Fig. 4 (a) J–V characteristics of $(FAPbI_3)_{0.85}(MAPbBr_3)_{0.15}$ solar cells. (b) The IPCE spectra and integrated current curves of $(FAPbI_3)_{0.85}(MAPbBr_3)_{0.15}$ solar cells. (c) The stabilized PCEs at the maximum power point. (d) The PCE distributions of 36 devices.

experimental J_{sc}. In order to evaluate the PSCs' photovoltaic performance, the stabilized power output of **SY1**, **SY2** and **SY3**-based PSCs devices is studied under maximum power point (MPP), as shown in Fig. 4c. **SY1**, **SY2** and **SY3**-based PSCs devices exhibited reliable high photovoltaic performances with stabilized PCEs of 17.08%, 18.24% and 18.95%, respectively, which agreed well with the obtained PCEs. The efficiency reproducibility of the PSCs devices based on these HTMs is shown in Fig. 4d. Average PCEs of 17.18%, 18.34% and 18.87% are achieved for the PSCs devices based on **SY1**, **SY2** and **SY3** with good reproducibility, respectively. These superior results suggest that D–π–D structured materials can serve as highly efficient HTMs for PSCs application.

To further evaluate the generality of **SY3** as a HTM in different PSCs, we also applied it as the HTM in all-inorganic PSCs with the optimized device configuration of ITO/SnO_2/ZnO_2/$CsPbI_2Br$/HTMs/MoO_3/Ag. The J–V curves are displayed in Fig. 5a and the photovoltaic parameters are listed in Table 2. The **SY3**-based $CsPbI_2Br$ PSCs produce a PCE of 13.41% with a J_{sc} of 14.93 mA cm^{-2}, a V_{oc} of 1.19 V and a FF of 0.755. The reference Spiro-OMe-TAD-based PSCs gives a PCE of 13.65%, with a J_{sc} of 15.01 mA cm^{-2}, a V_{oc} of 1.19 V, and a FF of 0.764. The corresponding IPCE spectrum of the best-performing PSCs devices are shown in Fig. 5b, wherein integrated J_{sc} values of 13.99 mA cm^{-2} and 13.65 mA cm^{-2} for **SY3** and Spiro-OMeTAD are achieved, respectively, which are in good agreement with the results obtained from the J–V curves.

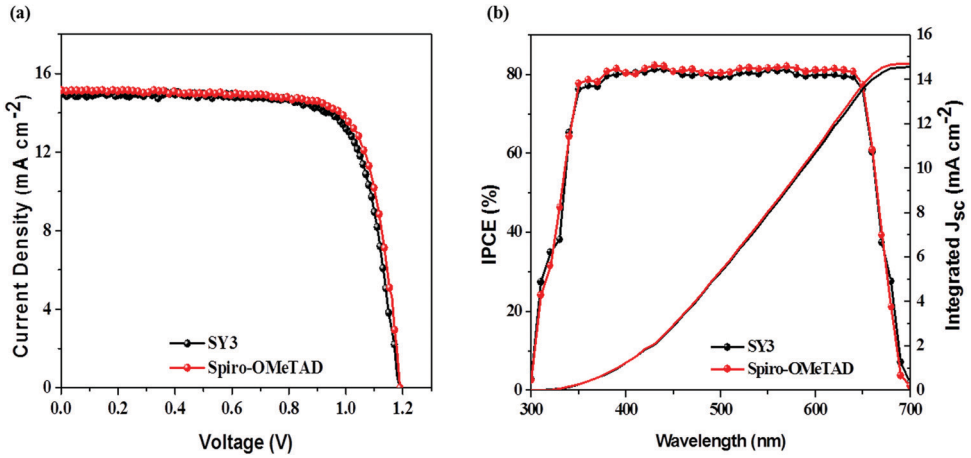

Fig. 5 (a) *J*–*V* characteristics of $CsPbI_2Br$ solar cells. (b) The IPCE spectra and integrated current curves of the $CsPbI_2Br$ solar cells.

Table 2 Photovoltaic parameters of PSCs based on **SY1**, **SY2**, and **SY3**

Perovskite	HTM	J_{sc} (mA cm^{-2})	V_{oc} (V)	FF (%)	PCE (%)
$(FAPbI_3)_{0.85}(MAPbBr_3)_{0.15}$	**SY1**	21.69	1.095	73.5	17.46
	SY2	22.55	1.099	74.6	18.49
	SY3	22.62	1.114	75.7	19.08
	Spiro-OMeTAD	22.75	1.123	76.1	19.44
$CsPbI_2Br$	**SY3**	14.93	1.19	75.5	13.41
	Spiro-OMeTAD	15.01	1.19	76.4	13.65

3.4. Surface morphology

A good morphological property with low surface roughness of HTM solid thin-film on a perovskite layer is very important for hole extraction and transfer at perovskite/HTM interface, which will benefit PSCs photovoltaic performance. Therefore, the surface morphology of HTMs films was characterized by using atomic force microscopy (AFM), as shown in Fig. 6a. Clearly, all of the three HTMs can form uniform and smooth films without small pinholes. The root mean-square (RMS) roughness values of **SY1**, **SY2** and **SY3** are 16.1 nm, 14.3 nm and 8.16 nm, respectively. In contrast, the **SY3** film shows less roughness than **SY1** and **SY2**, which helps to form an effective hole-selective contact between the perovskite layer and the Au electrode, resulting in a fast hole collection and transport in the PSCs devices.[47]

3.5. Steady-state and time-resolved photoluminescence and impedance spectroscopy studies

In order to investigate the extracting/transferring holes capability of the HTMs in devices, steady-state photoluminescence (PL) and time-resolved photoluminescence measurements (TRPL) were performed on the glass/perovskite/HTM. As shown in Fig. 6b, the PL emission of the pristine perovskite film is significantly quenched when these HTMs are deposited onto the surface of the perovskite layer, indicating that effective hole extraction happened at the perovskite/HTMs interfaces. The declined intensity of the PL emission followed the order of **SY3** > **SY2** > **SY1**, reflecting that **SY3** possesses a more efficient hole-extraction/transfer capability than **SY2** and **SY1** in PSCs devices. Notably, the **SY3**/perovskite bilayer shows quenching comparable with that of Spiro-OMeTAD, suggesting that **SY3** can extract/transport holes from perovskite as efficiently as Spiro-OMeTAD. Fig. 6c displays the TRPL spectra of perovskite with or without HTMs layer and the corresponding parameters are shown in Table S1 (ESI†). In the PL decay process, the short decay time (τ_1) can be attributed to the surface recombination and/or non-radiative recombination, while the long decay time (τ_2) might correlate with the bulk recombination. The perovskite layer coated with **SY3** gives a shorter PL decay lifetime (τ_1 6.84 ns, τ_2 25.24 ns) than that of **SY2** (τ_1 7.03 ns, τ_2 33.75 ns) and **SY1** (τ_1 9.95 ns, τ_2 55.53 ns). By contrast, the Spiro-OMeTAD/perovskite film shows τ_1 = 6.56 ns and τ_2 = 24.37 ns. These results further demonstrate the most efficient hole extraction/transfer capability of **SY3** as a HTM in PSCs, resulting in the corresponding better PSCs performance.[48] We further employ impedance spectroscopy to study the effect of HTM on the performance of PSCs. Fig. S8 (ESI†) shows Nyquist plots of PSCs with various HTMs under dark conditions. The figure shows a primary semicircle in the middle frequency region, which is attributed to the charge transport resistance (R_{rec}) in PSCs.[39] Generally, a higher R_{rec} reveals a more efficient charge extraction/transfer at the perovskite/HTM interface, suppressing effectively the charge recombination in the device. The **SY3**-based device exhibits a higher R_{rec} than the **SY1** and **SY2**-based ones, thus improving the device performance.

3.6. Device stability

To assess the effect of different HTMs on the device's long-term stability, aging tests were conducted at a relative humidity of

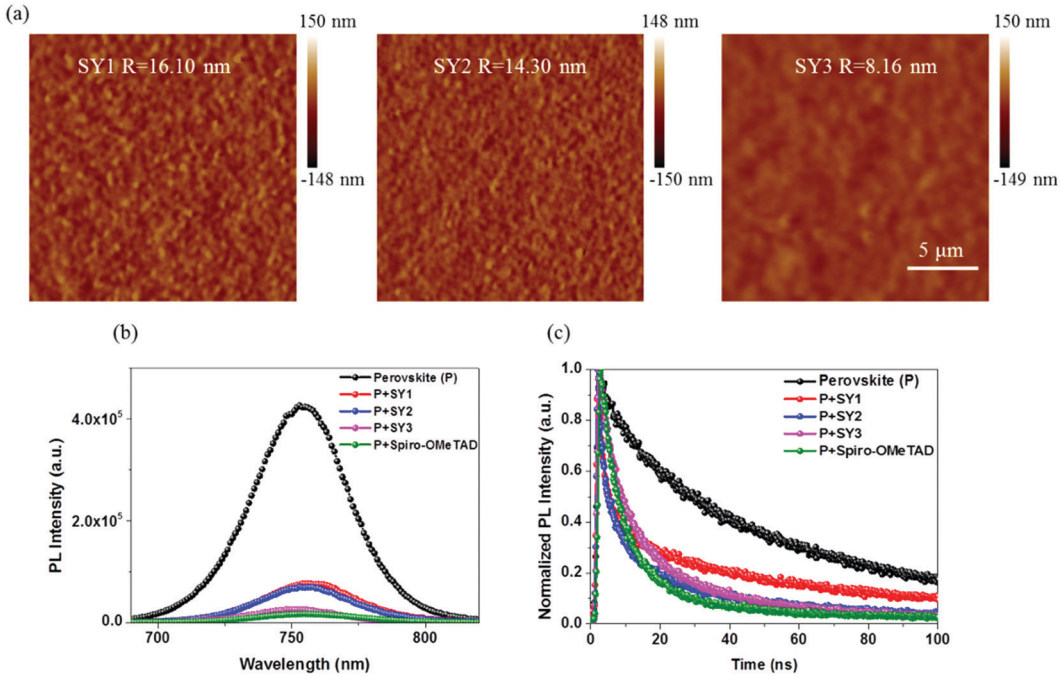

Fig. 6 (a) AFM height images for the HTM films. (b) Steady-state PL spectra of the perovskite films with and without HTMs. (c) Time-resolved PL decay of pristine perovskite film and perovskite/HTM films.

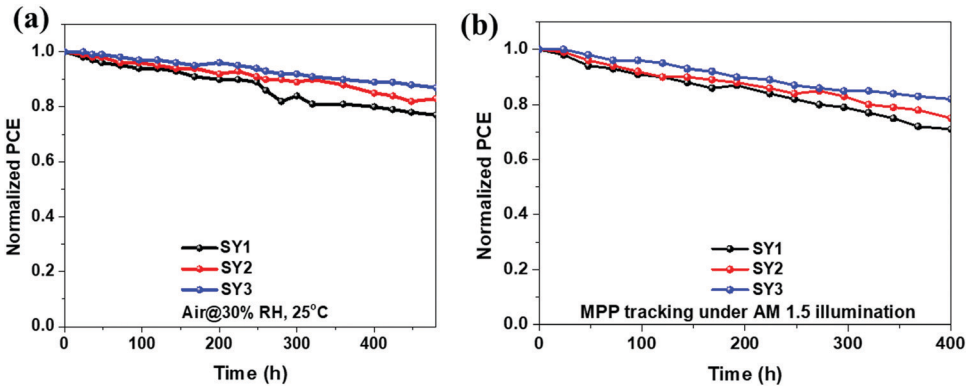

Fig. 7 (a) The stability of PSCs based on **SY1**, **SY2**, and **SY3** in air. (b) The stability of PSCs with **SY1**, **SY2**, and **SY3** under simulated solar illumination.

~30% without encapsulation and under continuous one-sun illumination at MPP. As shown in Fig. 7a, after 480 hours, the $(FAPbI_3)_{0.85}(MAPbBr_3)_{0.15}$ PSCs based on **SY3** showed the best long-term stability, only dropping to 87% of their starting efficiency, whereas the PCEs of **SY2** and **SY1**-based PSCs dropped to 82% and 76% under the same stored conditions, respectively. Fig. 7b shows that there is a 30%, 25% and 19% efficiency drop after 400 hour continuous one-sun illumination for **SY1**, **SY2** and **SY3**-based devices, respectively. To explain the difference in long-term stability, the water droplet contact angles on the surfaces of the three HTMs were performed. **SY1** and **SY2** exhibit a water contact angle of 65° and 72°, respectively, whereas the angle increases to approximately 84° for **SY3**. Thus, the higher hydrophobicity of **SY3** is extremely beneficial for enhancing the long-term stability of the PSCs. Moreover, the compact thin film of the **SY3** HTM could also act as a moisture barrier for the degradation of the perovskite layer under a humid environment.[49]

4. Conclusions

In summary, three D–π–D HTMs (**SY1**, **SY2**, and **SY3**), with diphenylamine as the donor along with a biphenyl, phenanthrene, or pyrene unit as the π-bridge, have been synthesized *via* a facile one-pot reaction and successfully applied in perovskite solar cells. The **SY3**-based hybrid $(FAPbI_3)_{0.85}(MAPbBr_3)_{0.15}$ PSCs afforded an impressive PCE of 19.08%, which is comparable to that of a cell fabricated with Spiro-OMeTAD (19.44%) and much better than the efficiencies of the **SY1** (17.46%) and **SY2** (18.49%)

based devices. Moreover, all-inorganic $CsPbI_2Br$-based PSCs with **SY3** as the HTM yielded a PCE of 13.41%. More importantly, the **SY3**-based PSCs without encapsulation display good long-term stability. This work shows that the introduction of larger π-conjugated bridges into HTMs could endow them with better hole extracting/transferring capabilities and better film-forming abilities. Our results provide valuable insight into the rational design of low-cost HTMs for use in highly efficient and stable PSCs in the future.

Conflicts of interest

The authors declare that they have no known competing financial interests or personal relationships that could have appeared to influence the work reported in this paper.

Acknowledgements

Y. Hua thanks the National Natural Science Foundation of China (22065038), the Key Project of Natural Science Foundation of Yunnan (KC10110419), the Fund for Excellent Young Scholars of Yunnan (K264202006820), the Program for Excellent Young Talents of Yunnan University and Major Science and Technology Project of Precious Metal Materials Genetic Engineering in Yunnan Province (No. 2019ZE001-1, 202002AB080001). L. Ding thanks the National Key Research and Development Program of China (2017YFA0206600) and the National Natural Science Foundation of China (51773045, 21772030, 51922032 and 21961160720) for financial support. H. B. Li thanks the fund of Young Scholars Program of Shandong University (Weihai), YSPSDUWH, and the Supercomputing Center, Shandong University, Weihai, for supercomputing system use.

References

1 N. J. Jeon, H. Na, E. H. Jung, T. Y. Yang, Y. G. Lee, G. Kim, H. W. Shin, S Il. Seok, J. Lee and J. Seo, A fluorene-terminated hole-transporting material for highly efficient and stable perovskite solar cells, *Nat. Energy*, 2018, **3**, 682–689.

2 M. M. Lee, J. Teuscher, T. Miyasaka, T. N. Murakami and H. J. Snaith, Efficient hybrid solar cells based on meso-superstructured organometal halide perovskites, *Science*, 2012, **338**, 643–647.

3 J. L. Yang, C. T. Zuo, Y. Peng, Y. (Michael) Yang, X. D. Yang and L. Ding, Large-area perovskite solar cells, *Sci. Bull.*, 2020, **65**, 872–875.

4 L. Shen, H. L. Yip, F. Gao and L. Ding, Semitransparent perovskite solar cells for smart windows, *Sci. Bull.*, 2020, **65**, 980–982.

5 M. Cheng, C. T. Zuo, Y. Z. Wu, Z. A. Li, B. M. Xu, Y. Hua and L. Ding, Charge-transport layer engineering in perovskite solar cells, *Sci. Bull.*, 2020, **65**, 1237–1241.

6 C. T. Zuo, D. Vaka, D. Angmo, L. Ding and M. Gao, One-step roll-to-roll air processed high efficiency perovskite solar cells, *Nano Energy*, 2018, **46**, 185–192.

7 K. Q. Huang, Y. Y. Peng, Y. X. Gao, J. Shi, H. Y. Li, X. D. Mo, H. Huang, Y. L. Gao, L. Ding and J. L. Yang, High-performance flexible perovskite solar cells via precise control of electron transport layer, *Adv. Energy Mater.*, 2019, **9**, 1901419.

8 A. Kojima, K. Teshima, Y. Shirai and T. Miyasaka, Organometal halide perovskites as visible-Light sensitizers for photovoltaic cells, *J. Am. Chem. Soc.*, 2009, **131**, 6050–6051.

9 M. Grätzel, The rise of highly efficient and stable perovskite solar cells, *Acc. Chem. Res.*, 2017, **50**, 487–491.

10 J. Burschka, N. Pellet, S. J. Moon, R. Humphry-Baker, P. Gao, M. K. Nazeeruddin and M. Grätzel, Sequential deposition as a route to high-performance perovskite-sensitized solar cells, *Nature*, 2013, **499**, 316–319.

11 Q. Jiang, Y. Zhao, X. Zhang, X. Yang, Y. Chen, Z. Chu, Q. Ye, X. Li, Z. Yin and J. You, Surface passivation of perovskite film for efficient solar cells, *Nat. Photonics*, 2019, **13**, 460–466.

12 S. Bai, P. Da, C. Li, Z. Wang, Z. Yuan, F. Fu, M. Kawecki, X. Liu, N. Sakai, J. T. Wang, S. Huettner, S. Buecheler, M. Fahlman, F. Gao and H. J. Snaith, Planar perovskite solar cells with long-term stability using ionic liquid additives, *Nature*, 2019, **571**, 245–250.

13 Q. Dong, Y. Fang, Y. Shao, P. Mulligan, J. Qiu, L. Cao and J. Huang, Electron-hole diffusion lengths >175 μm in solution-grown CH3NH3PbI3 single crystals, *Science*, 2015, **347**, 967–970.

14 S. D. Stranks, G. E. Eperon, G. Grancini, C. Menelaou, M. J. Alcocer, T. Leijtens, L. M. Herz, A. Petrozza and H. J. Snaith, Electron-hole diffusion lengths exceeding micrometer in an organometal trihalide perovskite absorber, *Science*, 2013, **342**, 341–344.

15 M. Liu, M. B. Johnston and H. J. Snaith, Efficient planar heterojunction perovskite solar cells by vapour deposition, *Nature*, 2013, **501**, 395–398.

16 H. R. Wang, H. Bian, Z. W. Jin, H. Zhang, L. Liang, J. L. Wen, Q. Wang, L. Ding, S. Zhong and F. Liu, Cesium lead mixed-halide perovskites for low-energy loss solar cells with efficiency beyond 17%, *Chem. Mater.*, 2019, **31**, 6231–6238.

17 S. Z. Wang, Y. Hua, M. K. Wang, F. Y. Liu and L. Ding, $CsPbI_{2.69}Br_{0.31}$ solar cells from low-temperature fabrication, *Mater. Chem. Front.*, 2019, **3**, 1139–1142.

18 Z. M. Fang, L. Liu, Z. M. Zhang, S. F. Yang, F. Y. Liu, M. Z. Liu and L. Ding, $CsPbI_{2.25}Br_{0.75}$ solar cells with 15.9% efficiency, *Sci. Bull.*, 2019, **64**, 507–510.

19 Z. M. Fang, X. Y. Meng, C. T. Zuo, D. Li, Z. Xiao, C. Y. Yi, M. K. Wang, Z. W. Jin, S. F. Yang and L. Ding, Interface engineering gifts $CsPbI_{2.25}Br_{0.75}$ solar cells high performance, *Sci. Bull.*, 2019, **64**, 1743–1746.

20 X. Jia, C. T. Zuo, S. X. Tao, K. Sun, Y. X. Zhao, S. F. Yang, M. Cheng, M. K. Wang, Y. B. Yuan, J. L. Yang, F. Gao, G. C. Xing, Z. H. Wei, L. J. Zhang, H. L. Yip, M. Z. Liu, Q. Shen, L. W. Yin, L. Y. Han, S. Z. Liu, L. Z. Wang, J. S. Luo,

H. R. Tan, Z. W. Jin and L. Ding, $CsPb(I_xBr_{1-x})_3$ solar cells, *Sci. Bull.*, 2019, **64**, 1532–1539.

21 G. Sathiyan, A. A. Syed, C. Chen, C. Wu, L. Tao, X. D. Ding, Y. W. Miao, G. Q. Li, M. Cheng and L. Ding, Dual effective dopant based hole transport layer for stable and efficient perovskite solar cells, *Nano Energy*, 2020, **72**, 104673.

22 C. Chen, C. Wu, X. D. Ding, Y. Tian, M. M. Zheng, M. Cheng, H. Xu, Z. W. Jin and L. Ding, Constructing binary electron transport layer with cascade energy level alignment for efficient $CsPbI_2Br$ solar cells, *Nano Energy*, 2020, **71**, 104604.

23 National Renewable Energy Laboratory, Best research-cell efficiencies chart, https://www.nrel.gov/pv/assets/pdfs/best-research-cell-efficiencies.20190802.pdf.

24 A. K. Jena, A. Kulkarni and T. Miyasaka, Halide perovskite photovoltaics: background, status, and future prospects, *Chem. Rev.*, 2019, **119**, 3036–3103.

25 J. U. Mora, I. G. Benito, A. M. Ontoria and N. Martin, Hole transporting materials for perovskite solar cells: a chemical approach, *Chem. Soc. Rev.*, 2018, **47**, 8541–8571.

26 C. C. Boyd, R. Cheacharoen, T. Leijtens and M. D. McGehee, Understanding degradation mechanisms and improving stability of perovskite photovoltaics, *Chem. Rev.*, 2019, **119**, 3418–3451.

27 Y. Hua, S. Chen, D. Y. Zhang, P. Xu, A. X. Sun, Y. M. Ou, T. Wu, B. Cui and X. J. Zhu, Bis[di(4-methoxyphenyl)-amino]carbazole-capped indacenodithiophenes as hole transport materials for highly efficient perovskite solar cells: the pronounced positioning effect of a donor group on the cell performance, *J. Mater. Chem. A*, 2019, **7**, 10200.

28 J. L. Wang, H. Zhang, B. X. Wu, Z. H. Wang, Z. Sun, S. Xue, Y. Z. Wu, A. Hagfeldt and M. Liang, Indeno[1,2-b]carbazole as methoxy-free donor group: constructing efficient and stable hole-transporting materials for perovskite solar cells, *Angew. Chem., Int. Ed.*, 2019, **58**, 15721–15725.

29 Z. Z. Li, F. G. Zhou, Q. Wang, L. Ding and Z. W. Jin, Approaches for thermodynamically stabilized $CsPbI_3$ solar cells, *Nano Energy*, 2020, **71**, 104634.

30 Y. H. Cheng, C. C. Xie, X. X. Liu, G. Y. Zhu, H. W. Li, S. Venkataraj, Z. K. Tan, L. Ding, A. G. Aberle and F. Lin, High-power bifacial perovskite solar cells with shelf life of over 2000 h, *Sci. Bull.*, 2020, **65**, 607–610.

31 S. Gangala and R. Misra, Spiro-linked organic small molecules as hole-transport materials for perovskite solar cells, *J. Mater. Chem. A*, 2018, **6**, 18750–18765.

32 Z. Hawash, L. K. Ono and Y. B. Qi, Recent advances in Spiro-MeOTAD hole transport material and its applications in organic-inorganic halide perovskite solar cells, *Adv. Mater. Interfaces*, 2018, **5**, 1700623.

33 T. P. I. Saragi, T. Spehr, A. Siebert, T. Fuhrmann-Lieker and J. Salbeck, Spiro compounds for organic optoelectronics, *Chem. Rev.*, 2007, **107**, 1011–1065.

34 J. Urieta-Mora, I. Garcia-Benito, A. Molina-Ontoria and N. Martin, Hole transporting materials for perovskite solar cells: a chemical approach, *Chem. Soc. Rev.*, 2018, **47**, 8541–8571.

35 B. Xu, J. B. Zhang, Y. Hua, P. Liu, L. Q. Wang, C. Q. Ruan, Y. Li, G. Boschloo, E. M. J. Johansson, L. Kloo, A. Hagfeldt, A. K. Y. Jen and L. Sun, Tailor-making low-cost Spiro-[fluorene-9,9'-xanthene]-based 3D oligomers for perovskite solar cells, *Chem*, 2017, **2**, 676–687.

36 M. Rumi, J. E. Ehrlich, A. A. Heikal, J. W. Perry, S. Barlow, Z. Y. Hu, D. M. Maughon, T. C. Parker, H. Röckel, S. Thayumanavan, S. R. Marder, D. Beljonne and J. Brédas, Structure-property relationships for two-photon absorbing chromophores: bis-donor diphenylpolyene and bis(styryl)-benzene derivatives, *J. Am. Chem. Soc.*, 2000, **122**, 9500–9510.

37 P. M. Beaujuge and J. M. J. Fréchet, Molecular design and ordering effects in π-functional materials for transistor and solar cell applications, *J. Am. Chem. Soc.*, 2011, **133**, 20009–20029.

38 D. Y. Zhang, P. Xu, T. Wu, Y. M. Ou, X. T. Yang, A. X. Sun, B. Cui, H. W. Sun and Y. Hua, Cyclopenta[hi]aceanthrylene-based dopant-free hole-transport material for organic-inorganic hybrid and all-inorganic perovskite solar cells, *J. Mater. Chem. A*, 2019, **7**, 5221–5226.

39 P. Xu, P. Liu, Y. Y. Li, B. Xu, L. Kloo, L. C. Sun and Y. Hua, D-A-D-Typed hole transport materials for efficient perovskite solar cells: tuning photovoltaic properties via the acceptor group, *ACS Appl. Mater. Interfaces*, 2018, **10**, 19697–19703.

40 Y. Hua, J. B. Zhang, B. Xu, P. Liu, M. Cheng, L. Kloo, E. M. J. Johansson, K. Sveinbjörnsson, K. Aitola, G. Boschloo and L. C. Sun, Facile synthesis of fluorene-based hole transport materials for highly efficient perovskite solar cells and solid-state dye-sensitized solar cells, *Nano Energy*, 2016, **26**, 108–113.

41 T. P. I. Saragi, T. Spehr, A. Siebert, T. Fuhrmann-Lieker and J. Salbeck, Spiro compounds for organic optoelectronics, *Chem. Rev.*, 2007, **107**, 1011–1065.

42 Y. Hua, B. Xu, P. Liu, H. Chen, H. N. Tian, M. Cheng, L. Kloo and L. C. Sun, High conductivity Ag-based metal organic complexes as dopant-free hole-transport materials for perovskite solar cells with high fill factors, *Chem. Sci.*, 2016, **7**, 2633–2638.

43 J. Zhang, Y. Hua, B. Xu, L. Yang, P. Liu, M. B. Johansson, N. Vlachopoulos, L. Kloo, G. Boschloo, E. M. J. Johansson and L. Sun, A. The role of 3D molecular structural control in new hole transport materials outperforming Spiro-OMeTAD in perovskite solar cells, Hagfeldt, *Adv. Energy Mater.*, 2016, **6**, 1601062.

44 Z. Yu and L. Sun, Recent progress on hole-transporting materials for emerging organometal halide perovskite solar cells, *Energy Mater.*, 2015, **5**, 1500213.

45 A. Krishna, D. Sabba, H. R. Li, J. Yin, P. P. Boix, C. Soci, S. G. Mhaisalkar and A. C. Grimsdale, Novel hole transporting materials based on triptycene core for high efficiency mesoscopic perovskite solar cells, *Chem. Sci.*, 2014, **5**, 2702–2709.

46 B. Xu, D. Bi, Y. Hua, P. Liu, M. Cheng, M. Grätzel, L. Kloo, A. Hagfeldt and L. Sun, A low-cost spiro[fluorene-9,9'-xanthene]-based hole transport material for highly efficient solid-state dye-sensitized solar cells and perovskite solar cells, *Energy Environ. Sci.*, 2016, **9**, 873.

47 H. Q. Lu, B. Z. He, Y. Ji, Y. H. Shan, C. Zhong, J. Xu, J. X. Liu, F. Wu and L. N. Zhu, Dopant-free hole transport materials

processed with green solvent for efficient perovskite solar cells, *Chem. Eng. J.*, 2020, **385**, 123976.

48 F. Liu, F. Wu, Z. Tu, Q. Liao, Y. Gong, L. Zhu, Q. Li and Z. Li, Hole transport materials based on 6,12-dihydroindeno[1,2-b]fluorine with different periphery groups: a new strategy for dopant-free perovskite solar cells, *Adv. Funct. Mater.*, 2019, **29**, 1901296.

49 K. A. Bush, C. D. Bailie, Y. Chen, A. R. Bowring, W. Wang, W. Ma, T. Leijtens, F. Moghadam and M. D. McGehee, Thermal and environmental stability of semi-transparent perovskite solar cells for tandems enabled by a solution-processed nanoparticle buffer layer and sputtered ITO electrode, *Adv. Mater.*, 2016, **28**, 3937.

